

# Variational quantum regression algorithm with encoded data structure

C.-C. Joseph Wang and Ryan S. Bennink

Quantum Computational Science Group, Quantum Information Science Section, Computational Sciences and Engineering Division, Oak Ridge National Laboratory, Oak Ridge, Tennessee 37831, USA

Variational quantum algorithms (VQAs) prevail to solve practical problems such as combinatorial optimization, quantum chemistry simulation, quantum machine learning, and quantum error correction on noisy quantum computers. For variational quantum machine learning, a variational algorithm with model interpretability built into the algorithm is yet to be exploited. In this paper, we construct a quantum regression algorithm and identify the direct relation of variational parameters to learned regression coefficients, while employing a circuit that directly encodes the data in quantum amplitudes reflecting the structure of the classical data table. The algorithm is particularly suitable for well-connected qubits. With compressed encoding and digital-analog gate operation, the run time complexity is logarithmically more advantageous than that for digital 2-local gate native hardware with the number of data entries encoded, a decent improvement in noisy intermediate-scale quantum computers and a minor improvement for large-scale quantum computing. Our suggested method of compressed binary encoding offers a remarkable reduction in the number of physical qubits needed when compared to the traditional one-hot-encoding technique with the same input data. The algorithm inherently performs linear regression but can also be used easily for nonlinear regression by building nonlinear features into the training data. In terms of measured cost function which distinguishes a good model from a poor one for model training, it will be effective only when the number of features is much less than the number of records for the encoded data structure to be observable. To echo this finding and mitigate hardware noise in practice, the ensemble model training from the quantum regression model learning with important feature selection from regularization is incorporated and illustrated numerically.

Regression models are predictive models that learn the map between a target continuous variable and predictors (attributes/input variables/features) in training. The predictor variables can generally be transformed into continuous ones with the appropriate interpretation based on the transformation performed. Regression models are important machine

C.-C. Joseph Wang and Ryan S. Bennink: [wangccj@ornl.gov](mailto:wangccj@ornl.gov), [benninkrs@ornl.gov](mailto:benninkrs@ornl.gov), This manuscript has been authored by UT-Battelle, LLC, under contract DE-AC05-00OR22725 with the US Department of Energy (DOE). The US government retains and the publisher, by accepting the article for publication, acknowledges that the US government retains a nonexclusive, paid-up, irrevocable, worldwide license to publish or reproduce the published form of this manuscript, or allow others to do so, for US government purposes. DOE will provide public access to these results of federally sponsored research in accordance with the DOE Public Access Plan (<https://www.energy.gov/doe-public-access-plan>).

learning models to study due to their wide adoption in industrial applications at scale, as opposed to more complex models such as neural networks, which typically focus on predicted results and less on understanding the correlation between the prediction outcomes and the predictors. Additional features, such as the flexibility to model nonlinear dependencies based on domain expertise and the ability to perform relevant variable selection with regularization techniques, further enhance the utility of regression modeling in statistical learning.

Model interpretability to boost explainability is essential for the wider adoption of machine learning applications, especially in domains where wrong model predictions can cause serious consequences. For example, in healthcare and financial applications, strict regulations require models with clear interpretation to validate model predictions, for the model to be approved/trusted. Model interpretability is an equally valid criterion for quantum machine learning but so far has received little attention. While a quantum regression algorithm was proposed a decade ago [1, 2, 3] and other approaches based on matrix inversion and quantum kernel methods have been proposed recently [4, 5], these works assumed noise-free quantum hardware and did not address model interpretation issues. Here we revisit quantum regression from a variational perspective with a known encoded data structure and develop an algorithm that provides interpretive value and prediction power as required to be useful in the noisy intermediate-scale quantum (NISQ) era [6]. In the NISQ era, variational quantum algorithms are undeniably the most feasible method [7, 8, 9, 10, 11]. They offer a practical solution to circumvent quantum hardware noises and intricate controls while maintaining their versatility for quantum computation [12].

We provide a different view to mitigating the scaling obstacles due to noise by ensemble regression learning with regularization. Regularization has been useful for resolving the well-known over-fitting problem in classical machine learning. While overfitting will likely not be a problem until quantum hardware noise is greatly suppressed, we show that regularization techniques can be a valid classical strategy for selecting important features in the context of the quantum algorithm.

## 1 Hybrid quantum regression algorithm

### 1.1 Problem statement

Regression is the task of determining the relationship between a set of independent quantities (or “features”)  $(X_1, \dots, X_M)$  and a dependent quantity (or “response”)  $Y$  from experimental data. It is one of the most common and important tasks in all science, with particular prevalence in data modeling and machine learning. Usually the relationship is assumed to be linear in  $X_m$ ,  $Y = \sum_{m=1}^M W_m X_m$  where  $(W_1, \dots, W_m)$  are known as regression coefficients or importance weights. However, by treating products of independent variables as additional independent variables, linear regression can also be used to model nonlinear relationships. In the typical regression scenario, one has  $L$  independent observations  $(y_0, \dots, y_{L-1})$  of  $Y$  and corresponding observations  $(x_{0m}, \dots, x_{(L-1)m})$  of each variable  $X_m$ . The goal of (linear) regression is to determine the coefficients  $(W_1, \dots, W_m)$  that best fit the data.

We propose a method to solve the linear regression problem using variational quantum circuits whose parameters encode the regression coefficients. The best regression coefficients are found by classical optimization with respect to a regularized cost function that furthermore helps to find the subset of features that are most important. A key aspect of our approach is that the structural data are encoded directly in the amplitudes of the

quantum state and the regression coefficients are encoded directly in the parameters of the quantum circuit, which leads to optimal interpretability. We note that protocols for implementing quantum amplitude encoding are still under active research [14, 15, 16]. Along with our regression algorithm, we provide several state preparation algorithms to facilitate the implementation of regression on near-term quantum computers.

## 1.2 Quantum amplitude encoding

The first step of our algorithm is to encode the observations  $y_0, \dots, y_{L-1}, x_{11}, \dots, x_{LM}$  in a quantum state. For notational convenience we define  $x_{l0} \equiv y_l$  and define  $\mathbf{X}$  as the matrix with elements  $\mathbf{X}_{lm} = x_{lm}$  for  $l = 0, \dots, L-1$  and  $m = 0, \dots, M$ . We begin by shifting and rescaling the data columnwise so that each column of  $\mathbf{X}$  has zero mean and equal variance. This ensures that our algorithm is equally sensitive to all variables for best training. Then the data is globally scaled so that  $\sum_{l,m} x_{lm}^2 = 1$ . (The scaling of the data must be accounted for when interpreting the regression coefficients obtained by the algorithm.) Therefore, the data can in principle be mapped to the amplitudes of a quantum state:

$$|\psi_D\rangle = \sum_{l,m} x_{lm} |lm\rangle \quad (1)$$

where  $\{|lm\rangle\}$  are computational basis states of a quantum system having at least  $L(M+1)$  orthogonal states. For now, we do not go into details about possible encoding schemes or methods of preparing  $|\psi_D\rangle$  so that we can illustrate the main ideas of the algorithm. Such details will be discussed in Section 2.

## 1.3 Mapping of regression coefficients to quantum amplitudes

Our goal is a variational circuit whose structure reflects that of the regression problem at hand and whose output is proportional to regression error

$$E = \sum_{l=0}^{L-1} (y_l - \tilde{y}_l)^2 \quad (2)$$

where

$$\tilde{y}_l = \sum_{m=1}^M x_{lm} W_m \quad (3)$$

is the predicted value of  $y_l$ .

We show first how to multiply a given feature (column of  $\mathbf{X}$ ) by a controllable coefficient. It will be convenient for exposition to treat the row index  $l$  and column index  $m$  as separate quantum degrees of freedom,  $|lm\rangle = |l\rangle \otimes |m\rangle \equiv |l\rangle|m\rangle$ . Consider the operator

$$U^{(m)}(\phi) = \mathbf{1} \otimes e^{-i\phi|m\rangle\langle m|} \quad (4)$$

which acts as identity (1) on the row (observation) register and imparts a phase to a selected element of the column (feature) register. It maps  $|l\rangle|m\rangle$  to  $e^{-i\phi}|l\rangle|m\rangle$  and leaves all other basis states unchanged. Thus when applied to  $|\psi_D\rangle$  it maps  $x_{lm} \rightarrow e^{-i\phi} x_{lm}$  for all  $l$ . By extension, the sequence  $\prod_{m=1}^M U^{(m)}(\phi_m)$  applies a controllable phase  $\phi_m$  to each column  $m$  of the data. In this case the resulting state would be

$$|\psi_D\rangle = \sum_{l,m} x_{lm} e^{-i\phi_m} |l\rangle|m\rangle. \quad (5)$$

Notice that the relation between  $\phi_m$  and the coefficient of  $|l\rangle|m\rangle$  is not exactly what we are looking for if we were to associate the phase  $\phi_m$  with the real regression parameters. The quantum map would not be real (up to a global phase factor) and is not linear in  $\phi_m$  as expected for conventional linear regression. Furthermore, the regression coefficients should range between  $[-\infty, +\infty]$  whereas the unique range of  $\phi_m$  is  $[-\pi, \pi]$ . Based on these observations we cannot make the direct association of the phases  $\phi_m$  with regression weights  $W_m$ . However if we engineer the circuit in a target code space to yield

$$|\psi_l\rangle \propto \sum_m x_{lm} (e^{-i\phi_m} + e^{+i\phi_m}) |l\rangle|m\rangle \propto \sum_m x_{lm} \cos \phi_m |lm\rangle \quad (6)$$

we can identify  $W_m \propto \cos \phi_m \in [-1.0, 1.0]$ , with the proportionality chosen to bring the weights into the needed range.

#### 1.4 Quantum regression algorithm

To engineer this mapping of phases to regression weights we use controlled phase gates of the form

$$U_C^{(m)}(\phi) = |0\rangle\langle 0| \otimes \mathbf{1} \otimes e^{i\phi_m|m\rangle\langle m|} + |1\rangle\langle 1| \otimes \mathbf{1} \otimes e^{-i\phi_m|m\rangle\langle m|} \quad (7)$$

which act on an ancilla qubit for control, row register, and column register respectively. (Note that if the hardware does not natively support such a controlled gate with symmetric phases, it can be realized as an *uncontrolled* rotation  $e^{i\phi_m}$  followed by a controlled rotation  $e^{-2i\phi_m}$ ). This gate imparts the phase  $e^{i\phi_m}$  to  $|0\rangle \otimes |l\rangle \otimes |m\rangle$ , imparts the phase  $e^{-i\phi_m}$  to  $|1\rangle \otimes |l\rangle \otimes |m\rangle$ , and leaves states with column index  $\neq m$  unchanged. As we now show, the transformation  $x_{lm} \rightarrow \cos \phi_m x_{lm}$  can be accomplished by such controlled phase gates with a suitably prepared and measured ancilla. The steps of the algorithm and corresponding evolution of the quantum state are:

1. Prepare the data state  $|\psi_D\rangle$ :

$$|\psi_D\rangle = \sum_{l,m} x_{lm} |lm\rangle \quad (8)$$

Ways of doing this will be discussed in Section 2.

2. Prepare an ancilla qubit in the state  $|+\rangle \equiv (|0\rangle + |1\rangle)/\sqrt{2}$ :

$$\longrightarrow |+\rangle \otimes |\psi_D\rangle. \quad (9)$$

3. Apply controlled phase gates  $U_C^{(m)}$  for each column  $m$ :

$$\longrightarrow \prod_m U_C^{(m)}(\phi_m) \left( \frac{|0\rangle + |1\rangle}{\sqrt{2}} \otimes |\psi_D\rangle \right) \quad (10)$$

$$= \frac{1}{\sqrt{2}} \sum_{l,m} (e^{i\phi_m} |0\rangle + e^{-i\phi_m} |1\rangle) \otimes x_{lm} |lm\rangle \quad (11)$$

4. Apply a Hadamard gate to the ancilla:

$$\longrightarrow \frac{1}{2} \sum_{l,m} (e^{i\phi_m} (|0\rangle + |1\rangle) + e^{-i\phi_m} (|0\rangle - |1\rangle)) x_{lm} |lm\rangle \quad (12)$$

$$= \frac{1}{\sqrt{2}} \sum_{l,m} (\cos \phi_m |0\rangle - i \sin \phi_m |1\rangle) x_{lm} |lm\rangle \quad (13)$$

5. Project the ancilla onto the state  $|0\rangle$ :

$$\longrightarrow |\Psi_0\rangle = \sum_{l,m} x_{lm} \cos \phi_m |lm\rangle \quad (14)$$

6. Measurement by the hermitian operator:

$$\hat{M} = \sum_{l=0}^{L-1} \sum_{m,m'=1}^M |lm\rangle \langle lm'|. \quad (15)$$

As shown in Appendix A, the expectation value  $\langle \hat{M} \rangle \equiv \langle \Psi_0 | \hat{M} | \Psi_0 \rangle$  is

$$\langle \hat{M} \rangle = \sum_{l=0}^{L-1} \left( \sum_{m=0}^{M+1} x_{lm} \cos \phi_m \right)^2 \quad (16)$$

$$= (\cos \phi_0)^2 \sum_l \left( y_l - \sum_{m=1}^M x_{lm} W_m \right)^2 \quad (17)$$

where we identify  $W_m = -\cos \phi_m / \cos \phi_0$  as the regression coefficient for feature  $m$  with  $M$  features and the response variable component  $y_l$  is by definition the  $x_{l0}$  component. With this identification the sum in the equation above can be recognized as the regression error (2). This result bridges the gap between our quantum regression algorithm and the conventional regression algorithm and enables clear interpretation of the variational parameters as discussed in our numerical studies. Although only the relative sign between the feature and response matters, we impose the condition  $\phi_y = \phi_0 \in (\frac{\pi}{2}, \frac{3}{2}\pi)$  so that  $\cos \phi_0$  is always negative and nonzero so that the regression coefficient  $W_m$  are well defined.

## 1.5 Model training and regularization

Since the goal is to minimize the regression error, the simplest approach is to take the cost function  $C(\mathbf{W})$  to be just the regression error  $E$ ,

$$C(\mathbf{W}) = \sum_{l=0}^{L-1} (y_l - \sum_{m=1}^M x_{lm} W_m)^2 = \frac{\langle \hat{M} \rangle}{(\cos \phi_0)^2} \quad (18)$$

where the regression weights  $\mathbf{W} = (W_1, \dots, W_m)$  are implicit functions of the circuit parameters  $\phi = (\phi_0, \dots, \phi_m)$ . The parameter vector  $\bar{\phi}$  that minimizes the cost function yields the optimal linear regression coefficients  $\bar{\mathbf{W}}$  with  $\bar{W}_m = -\cos \bar{\phi}_m / \cos \bar{\phi}_0$ . A fundamental question to ask is how sensitive the cost function is to a well-trained model as opposed to a poorly-trained model. When the data used to train the model is noise-free, we expect the cost function for a well-trained model to be zero. However, for a poor model, the cost function should be large enough to measure with significant probability. These details will be discussed in Appendix B.

In practice, regression typically includes regularization terms to bias toward models that fit the data well with fewer features, which helps avoid overfitting. The cost function is modified to

$$C(\mathbf{W}) = \sum_{l=0}^{L-1} \left( \sum_{m=1}^M x_{lm} W_m - y_l \right)^2 + \alpha \sum_{m=1}^M |W_m| + \beta \sum_{m=1}^M |W_m|^2. \quad (19)$$

where  $\alpha, \beta > 0$ . This cost function is given as a general elastic net regularization ( $\alpha \neq 0, \beta \neq 0$ ), which accommodates LASSO (least absolute shrinkage and selection operator,  $\alpha \neq 0, \beta = 0$ ) or Ridge ( $\beta \neq 0, \alpha = 0$ ) regularization as limiting cases. We note that the regularization terms can be evaluated on a classical computer and simply added to the cost function evaluated by the quantum computer.

With this general scheme, we can build our hybrid quantum-classical algorithm to find the best parameters  $\phi_m, \alpha, \beta$  which minimize the overall cost function. One would tend to implement the popular gradient-based approaches to search the minima. However, we do not consider this approach the best way forward for the following reasons. We expect landscapes with multiple vanishing gradients for our cost function due to the cosine functions for the phase angles and the optimization may end up with solutions far from optimal. In addition, the overhead in measurements protocol to extract gradient and Hessian matrix for the cost functions become the bottleneck for the overall hybrid quantum solutions. Instead, we employ the gradient-free Nelder-Mead (NM) optimization algorithm for the cost function to search the global minima. The downhill simplex method employed by NM may frequently be the best method to use if the figure of merit is “get something working quickly” for a problem whose computational burden is small [17]. We found convergence to the optimal value of the cost function to high accuracy typically can be found by passing the sub-optimal result from the latest global NM search as the starting parameter for the next global search iteratively until the desired accuracy is reached. When the model training involved a large amount of training data, the training can be broken down into ensemble training with multiple bootstrap data samples in parallel.

## 2 Implementation

Previously we have described how to implement the linear regression in a variational quantum circuit with controlled phase gates. To have an end-to-end solution, we need to consider how to encode the data in the quantum state, that is, how to prepare the data state  $|\psi_D\rangle$ . To that end we envision that the state can be prepared using programmable phase gates similar to those used to perform the regression. However, whereas in the regression step the phases depended only on the feature and were the same for each observation, to encode the data each a distinct phase  $\phi_{lm}$  will generally be needed for each data element  $x_{lm}$ . We notice that due to the global normalization condition, each normalized element  $x_{lm}$  is generally much smaller than 1. This indicates we can encode these classical data elements through small phase angles in which  $\sin x_{lm} \approx x_{lm}$ , that is, the phase angles are approximately the data elements themselves.

To minimize the potential hardware errors, we prefer low qubit counts while maintaining the simplicity of the algorithm. This is a particularly appealing solution for well-connected and programmable qubits such as Rydberg atom-based and ultra-cold ion quantum platforms [18, 19, 20]. At this point, we consider specifics of various encodings of the data.

### 2.1 One-hot encoding

#### 2.1.1 Data state preparation

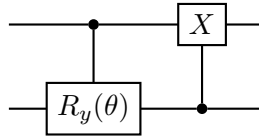
In one-hot encoding each pair  $(l, m)$  is mapped to a single index in  $\{1, \dots, L(M + 1)\}$  and encoded by a 1 value in the qubit with corresponding index. This would require  $L(M + 1)$  qubits. One-hot-encoding should be avoided for large data sets as it is resource hungry. For quantum machine learning on near-term quantum devices, this encoding is still useful

for the proof-of-concept of the algorithm we proposed since the circuits to implement it are relatively simple.

With one-hot encoding the pair  $(l, m)$  is mapped to a single index  $j = m + l(M + 1) \in \{0, \dots, L(M + 1) - 1\}$ . The basis state  $|lm\rangle$  is then encoded as  $|1_j\rangle \equiv |0\dots010\dots0\rangle$  which has 1 for qubit  $j$  and zero for every other qubit. This gives

$$|\psi_D\rangle = \sum_{l,m} x_{lm} |lm\rangle = \sum_{j=0}^{L(M+1)-1} x_j |1_j\rangle \quad (20)$$

We observe that a uniform superposition of one-hot-encoded states is the well-known  $W$  state that can be prepared by an efficient procedure [15]. The data state  $|\psi_D\rangle$  can be prepared using essentially the same procedure but with modified rotation angles to produce the generally nonuniform amplitudes  $x_j$ . The basic building block of this procedure is the gadget



consisting of a controlled- $Y$  rotation followed by a controlled-NOT gate. Such gates can be realized without difficulty in many experimental platforms (for example see Fig. 2 in the reference [20]). This gadget maps  $|10\rangle$  to  $\cos \theta |10\rangle + \sin \theta |01\rangle$ . Starting with the state  $|1_0\rangle = |10\dots0\rangle$  and applying this gadget with various angles to qubit pairs  $(0, 1), (1, 2), (2, 3), \dots$  one can prepare an arbitrary superposition of basis states  $|1_0\rangle, \dots, |1_{L(M+1)-1}\rangle$ . For typical digital two-local gates, the run time complexity scales as  $LM$  in the encoding. With programmable fully connected non-local gates, the run time complexity will be of order one.

### 2.1.2 Quantum regression map

In the one-hot encoding, the ancilla-controlled phase gate used to impart regression coefficients takes the form

$$U_C^{(j)}(\phi_j) = \exp(-i\phi_j |1\rangle\langle 1| \otimes |1_j\rangle\langle 1_j|) \quad (21)$$

$$= \exp\left(-i\phi_j \frac{Z_A - I_A}{2} \otimes \frac{Z_j - I_j}{2}\right) \quad (22)$$

where  $A$  denotes the ancilla,  $j$  indexes a data register qubit,  $Z_A$  ( $Z_j$ ) is the Pauli  $Z$  operator on qubit  $A$  ( $j$ ). It can be verified that  $U_C^j(\phi_j)$  yields the desired effect on  $x_j$  as  $U_C^j(|1\rangle \otimes |1_j\rangle) = \exp(-i\phi_j)(|1\rangle \otimes |1_j\rangle)$  and for every other state  $U_C$  acts as the identity. In Table 1, we summarize the full algorithm before measurement. The time complexity for the regression map will be further discussed in Appendix C.

### 2.1.3 Measurement

The measurement operator  $\hat{M}$  is the summation of individual operators of the form  $|lm\rangle\langle lm'|$ . This may be understood as a transition from  $j = (l, m)$  to  $j' = (l, m')$  which can be achieved by operators of the form  $S_{j'}^+ S_j^-$  where  $S_j^+ = |1\rangle\langle 0| = (X_j - iY_j)/2$  is the raising operator

Table 1: Summary of Quantum Algorithm with One-hot Encoding

| Summary of Quantum Algorithm with One-hot Encoding  |
|---|
| <b>Input:</b> The data registry state $ \psi_D\rangle$ is initialized as $W$ state with one-hot encoding $ A\rangle \otimes  \psi_D\rangle =  +\rangle \otimes \sum_{(l,m)} x_{lm}  lm\rangle$  |
| <b>Output:</b> The final quantum state before the projective measurement of the ancilla state $ 0\rangle$ : $ A\rangle \otimes  \psi_D\rangle = +\frac{1}{\sqrt{2}} [\sum_{l,m} x_{lm} \cos \phi_{lm}  0\rangle \otimes  lm\rangle - i x_{lm} \sin \phi_{lm}  1\rangle \otimes  lm\rangle]$                                     |
| <b>Procedure:</b>   |
| (1) Initialization of the ancilla state $ +\rangle$ and $W$ states for the data registry $ \psi_D\rangle$ .<br>(2) Application of multi-controlled phase gates with $\prod U_C^m$ .<br>(3) Application of a Hadamard gate $H$ to the ancilla $A$ .<br>(4) Projective measurement conditioned on the ancilla state $ 0\rangle$ . |

on qubit  $j$  and  $S_j^- = |0\rangle\langle 1| = (X_j + iY_j)/2$  is the lowering operator on qubit  $j$ .  $\hat{M}$  can be written in terms of measurable quantities as

$$\hat{M} = \sum_l \sum_{m,m'} |lm\rangle\langle lm'| \quad (23)$$

$$= I + \sum_l \sum_{m \neq m'} |lm\rangle\langle lm'| \quad (24)$$

$$= I + \sum_l \sum_{(j < k) = l(M+1)}^{l(M+1)+M} (S_j^+ S_k^- + S_k^+ S_j^-) \quad (25)$$

$$= I + \sum_l \sum_{(j < k) = l(M+1)}^{l(M+1)+M} (X_j X_k + Y_j Y_k), \quad (26)$$

where  $I$  denotes the global identity operator. Thus  $\hat{M}$  can be measured as a linear combination of  $I$ ,  $X_j X_k$ , and  $Y_j Y_k$  measurements.

Take a two-by-two data table for encoding as an example, the basis states for  $l = 0, m = 0, 1$  are  $|1000\rangle$  and  $|0100\rangle$ . For  $l = 1, m = 0, 1$ , the states are  $|0010\rangle$  and  $|0001\rangle$ . For  $l = 0$  the relevant state transition operators  $S_0^+ S_1^-$  and  $S_1^+ S_0^-$  are given by  $|1000\rangle\langle 0100|$  and  $|0100\rangle\langle 1000|$ . For  $l = 1$  the relevant state transition operators  $S_2^+ S_3^-$  and  $S_3^+ S_2^-$  are given by  $|0010\rangle\langle 0001|$  and  $|0001\rangle\langle 0010|$ .

One-hot amplitude encoding introduced so far can be resource intensive as the number of qubits scales with the number of classical data entries. However, the overall quantum algorithm is relatively simple. For the near-term hardware, we expect one-hot encoding to be the easiest to implement for proof-of-principle demonstrations of our algorithm. To mitigate hardware noise and reduce the size of quantum circuits needed a batch training strategy may be employed: One first divides the training data into much smaller batches of bootstrap samples and learns a regression model for each batch separately. Then the coefficients of the separate regression models are combined to yield an ensemble model, as will be demonstrated numerically in Section 3.

## 2.2 Compressed binary encoding

For the one-hot amplitude encoding, the allocated number of physical qubits to support the information grows linearly with the number of data entries. To extend the quantum algorithm for distributed big data applications for potential quantum advantages, we need to have a much more compact encoding scheme to minimize hardware noises due to a much larger qubit count for the same task. Meanwhile, we want to again keep the structure of the classical data table and use the simple ancilla-controlled phase gates.

Table 2: Summary of Quantum Algorithm with Compressed Binary Encoding

| Summary of Quantum Algorithm with Compressed Binary Encoding  |
|---|
| <b>Input:</b> The data registry state $ \psi_D\rangle$ is initialized as product state $ \mathbf{X}\rangle_{MEM}$ with binary encoding for each data element indexed by a value binary string.  |
| The ancilla is initialized in $ +\rangle$ state and the QPU register is initialized in a uniform superposition state $ \Psi\rangle$ with computational basis encoding a unique key for each data element at a different location of the data table. |
| <b>Output:</b> The final quantum state before projective measurement of the ancilla state $ 0\rangle$ .   |
| <b>Procedure:</b>   |
| (1) Initialization of the quantum state for the ancilla, data register and QPU register $ \Psi\rangle =  +\rangle \otimes \left(\frac{1}{\sqrt{K}} \sum_k  k\rangle_{QPU}\right) \otimes  \mathbf{X}\rangle_{MEM}$                                  |
| (2) Data state preparation by multi-controlled phase gates $\prod U_D^k$ operating on data register followed by projective measurement on the ancilla state $ -\rangle$ .   |
| (3) Unitary rotation of the ancilla from $ -\rangle$ state to $ +\rangle$ state.  |
| (4) Quantum regression map generation by multi-controlled phase gates $\prod U_C^m$ operating on QPU register.  |
| (5) Application of a Hadamard gate $H$ to the ancilla $A$ .   |
| (6) Projective measurement on the ancilla state $ 0\rangle$ .   |

For this encoding scheme the row and column information are stored in separate qubit registers,  $|lm\rangle = |l\rangle \otimes |m\rangle$ .  $l$  and  $m$  are each encoded in binary using  $N_L = \lceil \log_2 L \rceil$  qubits for  $l$  and  $N_M = \lceil \log_2(M+1) \rceil$  qubits for  $m$ . That is,  $|l\rangle = |l_{N_L}\rangle \otimes \cdots \otimes |l_1\rangle$  and  $|m\rangle = |m_{N_M}\rangle \otimes \cdots \otimes |m_1\rangle$ . Take for instance a  $4 \times 4$  data table representing 4 observations each of 3 features and 1 response variable. In this case the row index values  $l = 0, 1, 2, 3$  would be represented by the four basis states  $|00\rangle$ ,  $|01\rangle$ ,  $|10\rangle$ , and  $|11\rangle$ , respectively; the same four basis states in the column register would encode  $m = 0, 1, 2, 3$ .

Thus, the number of qubits needed to store the entire data table is approximately  $\log_2 L + \log_2 M = \log_2 LM$ , which represents a substantial compression. However, due to the compressed encoding, the procedure to impart the regression coefficients into the quantum state has a much higher complexity in terms of one- and two-qubit operations. Therefore, we will consider an alternative approach exploiting global entangling analog gates native to the latest cold-ion and Rydberg cold-atom systems.

### 2.2.1 State preparation

To prepare a quantum state  $|\psi_D\rangle$  containing the classical data  $\mathbf{X}$  in a binary encoding scheme, we consider the scheme in [14] in which the real data is first digitized and programmed into a computational basis state of quantum memory register. This need only be done once upfront. Subsequently, each time a copy of the quantum data state  $|\psi_D\rangle$  is needed, it is prepared by a fixed, efficient circuit that coherently applies phases stored in the quantum memory register to a quantum processing unit (QPU) register, without destroying the data in the memory register. The quantum information in the memory register can also be reinitialized when quantum coherence time is surpassed without changing the quantum algorithm in QPU.

We assign the index  $k = 0, \dots, K-1$  as the entries of a data table, where  $K = L(M+1)$ . Each data element  $x_k$  is digitized as  $\tilde{x}_k$  and stored in a separate qubit subregister (Fig. 1):

$$|\tilde{x}_k\rangle_{VAL[k]} . \quad (27)$$

To digitize  $x_k$ , let  $a$  be an upper bound on the magnitude of the data:  $\max_k |x_k| < a$  in which the magnitude of  $a$  is dependent on whether the data table is standardized and globally normalized or not before encoding. Then  $x_k \in [-a, a]$  is approximated using  $N_P$  bits of precision as

$$x_k \approx \tilde{x}_k = a \left( 2^{-1}(-1)^{x_{k,1}} + 2^{-2}(-1)^{x_{k,2}} + \cdots + 2^{-N_P}(-1)^{x_{k,N_P}} \right) \quad (28)$$

where  $x_{k,1}, \dots, x_{k,N_P} \in \{0, 1\}$ .  $\tilde{x}_k$  is then stored in the memory as

$$|\tilde{x}_k\rangle_{VAL[k]} = |x_{k,1}\rangle |x_{k,2}\rangle \cdots |x_{k,N_P}\rangle. \quad (29)$$

The full state of the memory register is

$$|\mathbf{X}\rangle_{MEM} = \bigotimes_{k=0}^{K-1} |\tilde{x}_k\rangle_{VAL[k]}. \quad (30)$$

The total number of qubits for the memory register is  $KN_P \approx LM \log_2(\epsilon^{-1})$  where  $\epsilon = 2^{-N_P}$  is the precision of each data element. While this the number of qubits is linear in the size of the data table, as noted above these qubits need only be kept in a classical digital state. Furthermore, the number of qubits can be reduced by using batching as previously discussed.

Once the data has been stored in the memory register, a fixed circuit uses the memory register coherently to impart the discrete data to amplitudes of the superposition state  $|\psi_D\rangle$  on the QPU register. We introduce an ancilla qubit in the state  $|+\rangle$  and an  $N_K$  qubit QPU register in a uniform superposition of all the binary encoded keys, yielding the state

$$|\Psi\rangle = |+\rangle \otimes \left( \frac{1}{\sqrt{K}} \sum_k |k\rangle_{QPU} \right) \otimes |\mathbf{X}\rangle_{MEM}, \quad (31)$$

in which the state  $|k\rangle_{QPU}$  is the shorthand for the encoded key  $|l\rangle|m\rangle$  for the data location in the table. Note that the QPU register size  $N_K = \lceil \log_2(L) \rceil + \lceil \log_2(M+1) \rceil \approx \log_2(LM)$  is much smaller than that of the (classical) memory register, which reduces opportunities for hardware errors. The essential step is a unitary which transfers the digitized classical data  $|\tilde{x}_k\rangle$  to the phase of the ancilla qubit when the key in the QPU register is  $k$  [14]:

$$U_D^k = \exp \left( -i Z_A \otimes |k\rangle \langle k|_{QPU} \otimes \hat{\theta}_k \right) \quad (32)$$

The operator  $\hat{\theta}_k$  is given by

$$\hat{\theta}_k = \sum_{j=1}^{N_P} \Delta\theta_j Z_{k,j} \quad (33)$$

in which  $Z_j^k$  is the operator on the  $j$ -th qubit on the value register  $|VAL\rangle[k]$ . When applied to the memory register,  $\hat{\theta}_k$  evaluates to the  $N_P$ -bit approximation to  $x_k$ :

$$\hat{\theta}_k |\mathbf{X}\rangle_{MEM} = \tilde{x}_k |\mathbf{X}\rangle_{MEM}. \quad (34)$$

Notice that the phase  $\Delta\theta_j = a2^{-j}$  is predetermined and can be realized by programming quantum gates with suitable gate times and interaction strengths, although fully programmable quantum hardware on a large scale is still an active research area in hardware implementation [20]. The factor  $|k\rangle \langle k|_{QPU}$  in the exponent causes this phase to be produced only if the state of the QPU register matches the key  $K$ . Explicitly,

$$U_D^k \left( |b\rangle_A \otimes |k'\rangle_{QPU} \otimes |\mathbf{X}\rangle_{MEM} \right) = e^{-i(-1)^b \tilde{x}_k \delta_{k,k'}} \left( |b\rangle_A \otimes |k'\rangle_{QPU} \otimes |\mathbf{X}\rangle_{MEM} \right) \quad (35)$$

where  $b \in \{0, 1\}$ . Then

$$\prod_k U_D^k |\Psi\rangle = \left( \frac{1}{\sqrt{K}} \sum_k \frac{e^{-i\tilde{x}_k} |0\rangle_A + e^{i\tilde{x}_k} |1\rangle_A}{\sqrt{2}} \otimes |k\rangle_{QPU} \right) \otimes |\mathbf{X}\rangle_{MEM}. \quad (36)$$

The encoded data state is then realized by projecting the ancilla qubit onto  $|-\rangle$ :

$$\langle -|_A \prod_k U_D^k |\Psi\rangle \propto \sum_k \sin \tilde{x}_k |k\rangle_{QPU} \otimes |\mathbf{X}\rangle_{MEM} \quad (37)$$

$$\approx |\psi_D\rangle_{QPU} \otimes |\mathbf{X}\rangle_{MEM} \quad (38)$$

since  $\sin \tilde{x}_k \approx \tilde{x}_k \approx x_k$  for a standardized data table.

The unitary  $U_D = \prod_k U_D^k$  is rather complex with terms involving many-qubit Pauli operators. Here we show that we can take advantage of nonlocal Mølmer-Sørensen gates which are available in current cold-ion technology [22, 21] and an active research area in Rydberg-atom platforms [18, 19]. We first expand the key selection operator in terms of Pauli strings and the binary encoding of  $k$  as  $k = k_{N_K} \cdots k_2 k_1$ :

$$|k\rangle \langle k|_{QPU} = \prod_{i=1}^{N_K} \frac{\mathbf{1} + (-1)^{k_i} Z_i^{QPU}}{2} \quad (39)$$

$$= 2^{-N_K} \sum_{P \in \{I, Z\}^{\otimes N_K}} (-1)^{\mathfrak{p}(P)} P_{QPU}, \quad (40)$$

Here  $\mathfrak{p}(P) \in \{0, 1\}$  is the parity of those bits of  $k$  that correspond to factors of  $Z$  in  $P$ . As a result,  $U_D^k$  can be written as  $U_D^k = \prod_{j=1}^{N_P} U_D^{k,j}$  where

$$U_D^{k,j} = \prod_{P \in \{I, Z\}^{\otimes N_K}} e^{-i2^{-N_K}(-1)^{\mathfrak{p}(P)} \Delta \theta_j Z_A \otimes P_{QPU} \otimes Z_{k,j}}. \quad (41)$$

Notice that each factor in  $U_D^{k,j}$  is a multiqubit Pauli rotation, where the operator in the exponent is a product of Pauli  $Z$  operators operating on selected qubits. It will soon be possible to implement such rotations efficiently in fully programmable cold ion or cold atom qubit architectures. As discussed in [22] and Appendix C of this paper, a many-qubit rotation can be realized by a short (length  $O(1)$ ) sequence of nonlocal Mølmer-Sørensen gates in conjunction with one-qubit ancilla gates on selected qubits. A basic MS operation generates a global set of pairwise interactions, while ancilla qubits in conjunction with MS operations generate interactions for Pauli strings on as many qubits as needed. We point out that this is an example of rarely-discussed digital-analog quantum computation [27]. In any case, the time complexity to implement  $U_D^k$  using such an approach is  $O(N_P 2^{N_K}) \approx N_P LM$ . There are  $LM$  keys, so the overall time complexity for state preparation  $\prod_k U_D^k$  goes as  $LM N_P 2^{N_K} \approx N_P (LM)^2$ .

In comparison, the cost of implementing  $U_D^{k,j}$  with digital local gates is greater. By the discussion of Hamiltonian simulation on page 210 of [25], the time complexity to implement a multiqubit rotation using local digital gates is roughly proportional to the number of qubits involved. Thus the time complexity to implement  $U_D^{k,j}$  using local digital gates is on the order of  $\sum_{n=1}^{N_K} n \binom{N_K}{n} = N_K 2^{N_K}$  with the overall time complexity  $\prod_{k,j} U_D^{k,j}$  estimated as  $LM N_P N_K 2^{N_K}$ . This is greater than the time complexity of the suggested global MS implementation by a factor of  $N_K \approx \log_2(LM)$ .

### 2.2.2 Quantum regression map

To impart the regression coefficients into the data state  $|\psi_D\rangle$  the memory register is not needed; the coefficients are imparted by the unitary  $U_C^m$ , Eq. (7), acting on the QPU and ancilla register:

$$U_C^m = e^{i\phi_m Z_A \otimes \mathbf{1} \otimes |m\rangle \langle m|}. \quad (42)$$

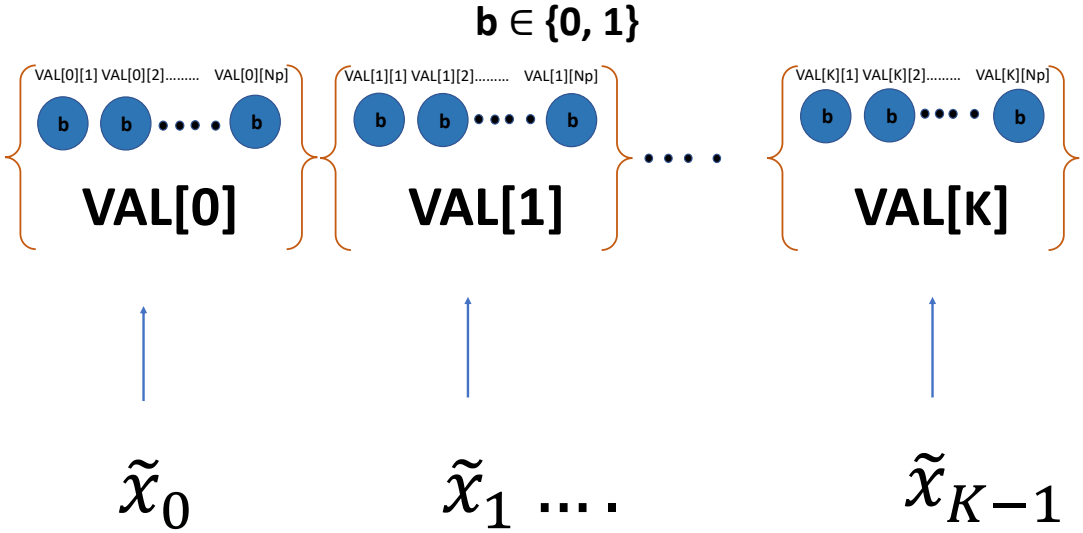


Figure 1: Quantum memory registry resource allocation: a physical qubit is represented by a filled circle with a binary code  $b \in \{0, 1\}$ .

$U_C^m$  is analogous to  $U_D^m$  but with two main differences. First, whereas  $U_D^k$  selects a specific data element  $k = (l, m)$ ,  $U_C^m$  selects only the column  $m$ , and performs identically on each row ( $l$ ) of the data table. The second difference is that whereas the phase imparted by  $U_D^k$  is encoded digitally in the quantum VAL register, the phase appearing in  $U_C^m$  is a simple scalar determined by the regression coefficient.

$U_C^m$  can be implemented using the same strategy as  $U_D^k$ . First, recall that the column index  $m$  is represented in binary as  $m = m_{N_M} \cdots m_2 m_1$  where  $N_M = \lceil \log_2(M+1) \rceil$ . Then

$$|m\rangle \langle m| = \otimes_{j=1}^{N_M} |m_j\rangle \langle m_j| = \prod_{j=1}^{N_M} \frac{\mathbf{1} + (-1)^{m_j} Z_j}{2} \quad (43)$$

where  $Z_j$  is the operator on  $j$ -th qubit in the  $|m\rangle$  subregister within the QPU register. Upon expanding the product  $U_C^m$  may be written as

$$U_C^m = \prod_{P \in \{I, Z\}^{\otimes N_M}} e^{+i(2^{-N_M} \phi_m(-1)^{\mathbf{p}(P)} Z_A \otimes \mathbf{1} \otimes P_{QPU})}, \quad (44)$$

where this time  $\mathbf{p}(P)$  is the parity of those bits of  $m$  that correspond to factors of  $Z$  in  $P$ . Again, these multiqubit rotations can be implemented either as a multi-qubit-controlled gate or using multi-qubit Mølmer-Sørensen gates as discussed above.

The time complexity for the feature mapping in quantum regression scales like  $2^{N_M} \times (M+1) \approx M^2$ . In Table 2, we summarize the full algorithm before measurement

### 2.2.3 Measurement

In the binary encoding, the measurement operator  $\hat{M}$ , Eq. (15) takes a particularly simple form:

$$\hat{M} = \sum_{l=0}^{L-1} |l\rangle \langle l| \sum_{m,m'=1}^M |m\rangle \langle m'|. \quad (45)$$

Using the binary expansion of  $|l\rangle$  we have  $\sum_l |l\rangle \langle l| = I^{\otimes N_L}$ . Similarly,  $\sum_{m,m'} |m\rangle \langle m'| = (2|+\rangle \langle +|)^{\otimes N_M} = (I + X)^{\otimes N_M}$ . Thus

$$\hat{M} = 2^{N_M} I^{\otimes N_L} \otimes (|+\rangle \langle +|)^{\otimes N_M} \quad (46)$$

$$= I^{\otimes N_L} \otimes (I + X)^{\otimes N_M} \quad (47)$$

Take a 2-by-4 data table for example. The  $|k\rangle$  states for  $l = 0$  are  $|0\rangle|00\rangle, |0\rangle|01\rangle, |0\rangle|10\rangle$ , and  $|0\rangle|11\rangle$ ; the states for  $l = 1$  are analogous. In this case

$$\hat{M} = I \otimes (I + X) \otimes (I + X) \quad (48)$$

$$= I \otimes I \otimes I + I \otimes I \otimes X + I \otimes X \otimes I + I \otimes X \otimes X. \quad (49)$$

$|\Psi_0\rangle = \psi_{000} |0\rangle|00\rangle + \dots + \psi_{111} |1\rangle|11\rangle$  denotes the state of the *QPU* register just prior to measurement. Then

$$\langle \hat{M} \rangle = |\psi_{000} + \psi_{001} + \psi_{010} + \psi_{011}|^2 + |\psi_{100} + \psi_{101} + \psi_{110} + \psi_{111}|^2. \quad (50)$$

In Appendix C, we discuss hardware implementation and resources for gate operation for interested readers.

### 3 Numerical results

Conventionally, to draw reliable interpretations from a trained regression model, we need to characterize the statistics of the uncertainty for the corresponding regression parameter for the predictor variables to justify its relevance in explaining the data. Motivated by the bootstrap aggregation (bagging) in the success of the random forest algorithm, we can build a regression model with bootstrap samples and compute the average and the standard errors (SEs) of the predicted regression coefficients by drawing the same number of data records from the bootstrapped samples from the original master (data) population (See reference [26] for advanced statistical concepts and practical numerical analysis). Since the qubits in quantum hardware would be noisy to handle a big data set, a plausible solution is to train the regression model from smaller bootstrap samples (bagging) from the smaller subsets of the training data with the same circuit to quantify errors and gather the final bootstrap statistics of the regression parameters by averaging the measurement results from the quantum algorithm running by the quantum hardware. In another vein, the traditional statistical model approaches in data science should be generalizable to hybrid quantum machine learning as illustrated in the following numerical demonstration as an example. The generalization and extension to other quantum machine models are required to explore further.

Here we show the promise of quantum encoded data that can be processed in well-connected quantum hardware and provide an alternative hybrid quantum solution for quantum machine learning applications. For the proposed variational quantum regression (VQR), we show a different and robust strategy to use a global optimization search algorithm to find the optimal regression coefficients to avoid measurement overheads based on gradient-based approaches. The best estimation can be found by using the sub-optimal solutions with lower accuracy for regression coefficients as a new ansatz initialization for the next round of global Nelder-Mead (NM) optimization algorithm until the final converged solution to high accuracy is found. For numerical demonstration, we adopt the NM optimization algorithm from SciPy (an open-source Python library for scientific and technical computing) to validate the batch learning strategy with the analytically-known

cost function in Eq. (17) (for big data application with bootstrap samples, one should survey the NM optimizers provided by Tensorflow or Pyspark: the algorithm provided can be utilized to save time with high performance computation). In the following numerical results, the tuning variables for the cost function are cosine functions for the phase angles instead of phase angles. The search for our optimal solutions is more effective from the new variables because of the unconstrained search for the NM optimizer.

### 3.1 Ensemble model training

Machine learning from an ensemble model can be useful for statistical modeling so that it is scalable with large data. We trained an ensemble model from  $N_b$  sets of bootstrap samples of various sizes. The best model is determined by the estimated weight vector  $\tilde{\mathbf{W}}$  calculated from the estimated feature weights  $\tilde{\mathbf{W}} = (\tilde{W}_1, \tilde{W}_2, \dots, \tilde{W}_M)$  from bootstrap samples, that is,  $\tilde{W}_i = N_b^{-1} \sum_{b=0}^{N_b-1} \tilde{W}_i^b$  in which  $\tilde{W}_i^b$  is the weight learned from the batch  $b$  for the feature  $i$  and the standard errors (SEs) for the weights from model training is denoted as  $\delta \tilde{W}_i$ .

To validate the ensemble learning, we generate synthetic and standardized classical data sets with a deterministic linear map with small randomness between the  $M$  features  $X_j = (X_{j,1}, X_{j,2}, \dots, X_{j,M})$  and the target variable  $Y_j \in R$ . Specifically, the ideal (noiseless) linear map is given by the expression  $Y_j = X_{ji} \bar{W}_i$  where  $X_{ji}$  is the  $L$ -by- $M$  data matrix and the best weight vector  $\bar{\mathbf{W}} = (\bar{W}_1, \bar{W}_2, \dots, \bar{W}_M)$  of size  $M$  after data standardization. We let each feature follow the uniform random distribution between values  $[-1, 1]$  to cover the feature space. For the response column  $Y_j$ , it is generated by the linear map  $Y_j = X_{ji} W_i$  with the random variables  $\{W_{i=1,2,\dots,M}\}$  with the ideal population mean  $\bar{\mathbf{W}} = (\bar{W}_1 = 1.0, \bar{W}_2 = 2.0, \bar{W}_3 = 3.0, \dots, \bar{W}_M = \text{float}(M))$  and the standard deviation  $\delta$  (the same for each feature) from its mean value  $\bar{W}_i$ . We would expect the model training would be more uncertain for the first few features due to the smaller signal-to-noise ratio  $\tilde{W}_i / \delta \tilde{W}_i$  where  $i = 1, 2, \dots, M$  from an equal number of bootstrap samples with different sample sizes. Notice that the weights  $\tilde{W}_i$  and the SEs  $\delta \tilde{W}_i$  from training are in tilde to differentiate from the mean weight  $\bar{W}_i$  and the standard deviation  $\delta$  from the data generation respectively.

| Sample size | $\tilde{W}_1$ | $\tilde{W}_2$ | $\tilde{W}_3$ | $\tilde{W}_4$ | $\tilde{W}_5$ | $\tilde{W}_6$ |
|-------------|---------------|---------------|---------------|---------------|---------------|---------------|
| 10          | 0.99938       | 2.00113       | 2.99967       | 3.99968       | 5.00004       | 6.00009       |
| 20          | 1.00008       | 2.00004       | 3.00002       | 4.00001       | 5.00002       | 5.99998       |
| 40          | 1.00004       | 2.00007       | 3.00003       | 4.00013       | 5.00000       | 6.00012       |
| 60          | 0.99999       | 2.00001       | 2.99998       | 4.00006       | 5.00001       | 6.00004       |
| 100         | 1.00001       | 2.00001       | 3.00004       | 4.00002       | 5.00000       | 6.00002       |
| 150         | 0.99997       | 2.00001       | 3.00002       | 4.00001       | 5.00004       | 6.00002       |

Table 3: Weight Vector for different bootstrap sample sizes without population noise

A bootstrap sample is a sampled data set that is drawn with the replacement from the original master population. For our numerical demo, the master population data set has  $N_b = 1024$  data records/rows and we drew 1024 bootstrap samples, each of which has a much smaller chosen sample size. The regression weight vector learned by the proposed regression algorithm from the 1024 bootstrap re-samples with the respective sample sizes 10, 20, 40, 60, 100, and 150 records. The zero bias term is guaranteed to be negligible from data standardization due to subtraction from the sample mean. Including additional columns from the response variable for the quantum encoding, we can emulate classically the quantum regression training with 13 qubits ( $2^{13} = 1024 \times 7$ ) without padding additional

| Sample size | $\delta\tilde{W}_1$ | $\delta\tilde{W}_2$ | $\delta\tilde{W}_3$ | $\delta\tilde{W}_4$ | $\delta\tilde{W}_5$ | $\delta\tilde{W}_6$ |
|-------------|---------------------|---------------------|---------------------|---------------------|---------------------|---------------------|
| 10          | 0.02039             | 0.03495             | 0.00725             | 0.01284             | 0.00934             | 0.00781             |
| 20          | 0.00204             | 0.00118             | 0.00156             | 0.0016              | 0.00154             | 0.00217             |
| 40          | 0.00153             | 0.00316             | 0.003               | 0.00299             | 0.00155             | 0.00245             |
| 60          | 0.00077             | 0.00072             | 0.00076             | 0.00172             | 0.00056             | 0.00088             |
| 100         | 0.00087             | 0.00104             | 0.00106             | 0.00074             | 0.00092             | 0.00174             |
| 150         | 0.00069             | 0.00052             | 0.00049             | 0.00034             | 0.0009              | 0.00079             |

Table 4: SEs of weight vectors for different bootstrap sample sizes without population noise

| Sample size | $t_1$      | $t_2$      | $t_3$      | $t_4$       | $t_5$      | $t_6$      |
|-------------|------------|------------|------------|-------------|------------|------------|
| 10          | 49.0036    | 57.25731   | 413.59599  | 311.55844   | 535.45297  | 768.20304  |
| 20          | 490.03614  | 1697.92281 | 1924.45761 | 2506.22625  | 3237.56853 | 2759.18714 |
| 40          | 653.08249  | 632.31813  | 1000.64225 | 1339.80026  | 3227.4301  | 2453.23403 |
| 60          | 1291.6086  | 2787.94434 | 3970.08524 | 2321.44326  | 8930.72652 | 6798.62171 |
| 100         | 1152.23006 | 1930.15583 | 2824.33706 | 5433.56226  | 5444.65661 | 3455.64034 |
| 150         | 1457.42293 | 3855.09323 | 6125.15592 | 11916.92773 | 5580.49053 | 7587.86445 |

Table 5: SEs of weight vectors for different bootstrap sample sizes without population noise

zeros.

Due to the variance of the bootstrap samples, the trained weight vectors fluctuate among these samples. To establish our baseline errors from sampling and training, we show the ideal case with six features where the training data has no noise  $\delta = 0$  to see if we can emulate the learning. As shown in Table 3, the training reproduces the theoretical values for the synthetic data we generate with the ideal weight vector  $\bar{\mathbf{W}} = (1.0, 2.0, 3.0, 4.0, 5.0, 6.0)$  and we observe that the bootstrap sampling for the learning is reproduced for various batch sizes. SEs of the weight vector  $\delta\bar{\mathbf{W}} = (\delta\tilde{W}_1, \delta\tilde{W}_2, \dots, \delta\tilde{W}_6)$  stay small and almost unchanged for different batch sizes as shown in Table 4. With the SEs in weight staying more or less constant, we expect a much larger  $t$  for the features with higher weights. If we look at the  $t$ -statistics metrics defined by the ratio  $t_i = \tilde{W}_i/\delta\tilde{W}_i$  as shown in Table 5, we observe these values are much greater than one representing the statistical significance of the learned results. This shows that bootstrap sampling analysis is a valuable tool and generalizable in practice beyond Gaussian noise hypothesis [26], typically imposed in traditional statistical analysis.

To further confirm the practicality of the training approach with noise present in the map between features  $X_i$  and the response variable  $Y_i$ , we go through the simulation with the noise level  $\delta = 0.1$ . For this case, we observe the deviation of the learned weight vectors away from the ideal case without noise. With small sample sizes 10, 20, and 40, the sample mean weights can deviate from the theoretical weight vector more than what is indicated by the noise  $\delta = 0.1$  in Table 6. This is due to the sample variance is more pronounced at smaller batch sizes as indicated in noiseless case  $\delta = 0$  in Table 4.

For the larger sample sizes 60, 100, and 150, we do observe the mean weight vector from training mostly reproduce what is expected for the noise level  $\delta = 0.1$ . The SEs of the weight vectors for the noisy cases is shown in Table 7. When the learned weight vectors significantly deviate from theoretical values, we observe a corresponding larger SE for the weight vector. This correlation gives us guidance on how reliable our learned weight vectors are. For example, for the first feature  $\tilde{W}_1$  with the sample size 20, we see a large deviation from the theoretical value  $1 \pm 0.1$ . We also observe a larger deviation in its SE:  $\delta\tilde{W}_1$  at the

sample size 20. In Table 8, we observe the overall  $t$  values are lower in comparison with the cases with no noise  $\delta = 0$  due to the presence of non-sampling noise. In addition, we can identify the overall  $t$  values are the largest for the batch size 150. This indicates that we can use bootstrap sampling with the optimal sample size of 150.

For larger batch sizes greater than 150 (not shown), we start to observe the deviation from what we expect from theoretical values for the weight vector  $\bar{\mathbf{W}}$ . This is due to the fact that the ensemble training from the resample data sets is under-fitting due to higher chances of duplicated data records in each sample, leading to the training bias. Even though the bias hinders us to draw quantitative inferences from the data, this behavior does not prevent us from selecting important features based on the  $t$ -statistics metrics defined by the ratio  $t_i = \bar{W}_i / \delta \bar{W}_i$  as shown in Table 8 and can be avoided with smaller bootstrap sample size. Note that this is also the case when there is no noise  $\delta = 0$  (Table 5) but occurs at a larger batch size  $> 150$  not shown in Table 3.

| Sample size | $\tilde{W}_1$ | $\tilde{W}_2$ | $\tilde{W}_3$ | $\tilde{W}_4$ | $\tilde{W}_5$ | $\tilde{W}_6$ |
|-------------|---------------|---------------|---------------|---------------|---------------|---------------|
| 10          | 1.24838       | 2.01457       | 2.92003       | 3.85253       | 4.69864       | 5.62674       |
| 20          | 0.02961       | 2.66497       | 1.64403       | 3.86877       | 5.15871       | 5.44711       |
| 40          | 1.80006       | 0.74388       | 2.9371        | 3.97106       | 5.45333       | 5.65369       |
| 60          | 0.89376       | 1.83072       | 2.97385       | 4.07048       | 4.74884       | 5.72274       |
| 100         | 0.63928       | 1.19575       | 3.04848       | 3.61821       | 5.09804       | 6.29805       |
| 150         | 1.14361       | 1.79783       | 2.8523        | 3.95466       | 4.75087       | 5.82112       |

Table 6: Weight vectors for different bootstrap sample sizes with Gaussian noise  $\delta = 0.1$

| Sample size | $\delta \tilde{W}_1$ | $\delta \tilde{W}_2$ | $\delta \tilde{W}_3$ | $\delta \tilde{W}_4$ | $\delta \tilde{W}_5$ | $\delta \tilde{W}_6$ |
|-------------|----------------------|----------------------|----------------------|----------------------|----------------------|----------------------|
| 10          | 10.3005              | 12.11829             | 13.45395             | 10.91457             | 7.85075              | 15.71212             |
| 20          | 18.87171             | 28.18201             | 32.64924             | 14.18558             | 18.51711             | 21.57881             |
| 40          | 16.54549             | 46.15104             | 6.43802              | 17.95377             | 20.97624             | 8.10855              |
| 60          | 5.92399              | 5.39804              | 7.86823              | 6.12054              | 7.67524              | 5.49687              |
| 100         | 9.85255              | 17.82527             | 8.84548              | 19.16585             | 10.84676             | 9.2562               |
| 150         | 3.92479              | 3.14805              | 2.88643              | 3.30615              | 3.54041              | 3.47353              |

Table 7: SEs of the weight vectors for different bootstrap sample sizes with Gaussian noise  $\delta = 0.1$

| Sample size | $t_1$   | $t_2$   | $t_3$   | $t_4$   | $t_5$   | $t_6$   |
|-------------|---------|---------|---------|---------|---------|---------|
| 10          | 0.1212  | 0.16624 | 0.21704 | 0.35297 | 0.5985  | 0.35811 |
| 20          | 0.00157 | 0.09456 | 0.05035 | 0.27273 | 0.27859 | 0.25243 |
| 40          | 0.10879 | 0.01612 | 0.45621 | 0.22118 | 0.25998 | 0.69725 |
| 60          | 0.15087 | 0.33915 | 0.37796 | 0.66505 | 0.61872 | 1.04109 |
| 100         | 0.06488 | 0.06708 | 0.34464 | 0.18878 | 0.47001 | 0.68041 |
| 150         | 0.29138 | 0.57109 | 0.98818 | 1.19615 | 1.3419  | 1.67585 |

Table 8: Bootstrap-statistics metrics for the weight vectors for different bootstrap sample sizes with Gaussian noise  $\delta = 0.1$

### 3.2 Feature importance and regularization

In machine learning, we may have a potentially large list of features that can be used to describe the mapping between the response variable and input variables. Regularization provides an algorithmic way to select the optimal subset of original features quickly before doing a more detailed bootstrap sampling analysis for the finalized features. Regularization penalizes the model with many features with important weights to avoid over-fitting the noise present in the training data that is relevant in noisy hardware and avoids dependent predictors entering the built models. Since the regularization is done outside the quantum loop, this is a valid strategy for hybrid quantum machine learning. Here we demonstrate that the optimal feature selection can be enabled by turning on regularization in the cost function. To establish the baseline, we generate synthetic data without Gaussian noises  $\delta_0 = 0$  where the response variable  $Y = \sin(x)$  depends on the independent real variable  $x$  in infinite order and the values distribute randomly between the values  $[-1, 1]$ . This is an infinite series for any real  $x$  values but can be truncated to a finite series when  $x$  ranges between  $[-1, 1]$ , which is the case for our normalized features. For regularization, we test with  $L1$  regularization and  $L2$  regularization. We found the  $L1$  regularization works robustly with the NM optimization algorithm in this case.

In the following demonstration, we show that the nonlinear features can be built first in the feature so that the linear regression algorithm can be used for the nonlinear regression model building. We generate the synthetic data with controlled mapping between predictors (features)  $\mathbf{X} = (X_1 = x, X_2 = x^2, X_3 = x^3, \dots, X_{15} = x^{15})$  and the target (response) variable  $Y \in R = \sin(x) = \sum_{n \in +\mathbb{Z}} (-1)^{n+1} x^{2n-1} / (2n-1)!$ . The number of population records  $2^5$  are generated where each feature  $X_n$  is uniformly generated between values  $[-1, 1]$ . With  $L1$  regularization, we use the very small regularization parameter  $\alpha = 1.2 \times 10^{-7}$  and alternating signs for the initial weight ansatz as,  $\text{sign}(W_1, W_3, W_5, \dots, W_{15}) = (+1, -1, +1, \dots, -1)$ . Our hybrid algorithm converges to the optimal weight parameter  $\widetilde{\mathbf{W}} \approx \overline{\mathbf{W}}$ , which selects the first few odd terms as the important features. Noticed that the optimization may end up with a much smaller cost function but with the wrong signs. However, this confirms the experience that constraints from domain knowledge typically are required since the classical optimization algorithms can only be used as a filter for possible solutions and even a mathematical global minimum solution may not be reasonable for the domain of applications. What we found is that  $L1$  regularization works with the proper regularization parameters  $\alpha$ . The number of vanishing weights in the converged weight vector reveals itself to enable the feature selection effectively. Take the best-learned weight to produce the predicted value  $Y$  for  $x$  values ranging between  $[-1, 1]$  as shown in Figure 2, we can reproduce what we expected from synthetic training data.

## 4 Conclusion

To conclude, our work significantly bridges the gap between the quantum algorithm and the regression modeling in quantum machine learning through the explicit interpretation of relevant model parameters from the physical parameters of qubit resources used for structural encoding. We have prescribed a hybrid VQA for quantum regression modeling and discussed its time complexity. The proposal is particularly suited for a quantum platform with well-connected qubits as resources such as cold atoms and ions. In addition, we elucidate the roles regression coefficients(weights) played in the model, which is connected to the ratio of cosine functions of phase angles between amplitude-encoded states assigned

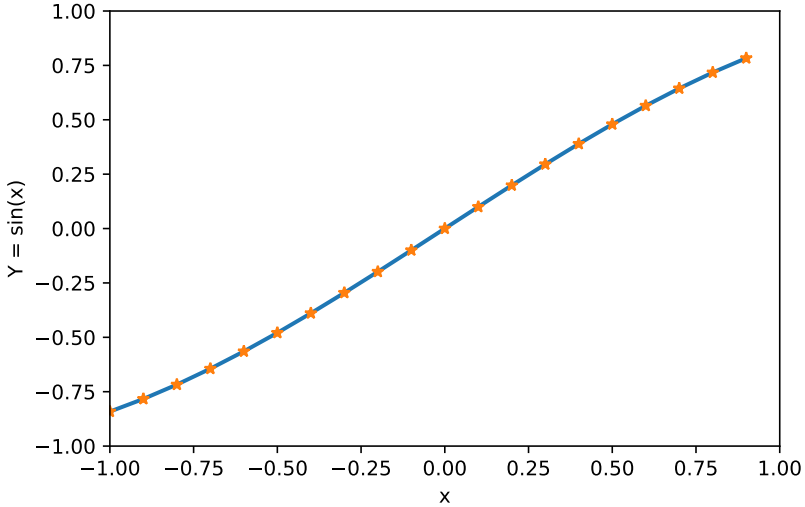


Figure 2: Prediction Agreement with theory and the weights from training are truncated to the fourth accuracy decimals  $\bar{\mathbf{W}} = (0.9992, 0.000001435, -0.1629, -0.000002908, 0.004134, -0.0004442, 0.000004760, 0.0000012079, 0.000005189, 0.0003221, 0.0008932, 0.0001738, 0.000001149, -0.000001869, -0.000001375)$ .

between the features and the response variable in the original tableau. For well-known linear inversion problems for optimal physical modeling, our hybrid quantum algorithm can also be applied if proper normalization is accounted for with care.

For near-term hardware with limited quality qubits, we investigate an alternative ensemble training solution and provide numerical evidence for the feasibility of the strategy. We show the  $t$  statistics to characterize the reliability of the learned weight coefficient versus its standard error. For the training tasks with enormous features to select for model training, we suggest that  $L1$  regularization can be a valid tool external to the variational quantum state ansatz when it is too expressive. To enable the realization of our algorithm in hardware, we recommend the simple one-hot amplitude encoding for small training data sets for its less stringent technical requirement for hardware. In conjunction with ensemble learning, the hybrid machine-learning solution can scale in time. For less noisy and well-connected computing hardware, compressed amplitude encoding should be more advantageous, in synchronous with the very rapid development of cold atom platforms. As we have learned in the algorithm design, it appears more advantageous to have a quantum algorithm designed with digital local and global gates present in NISQ hardware for improved time complexity and reduced qubit resources beneficial for noise mitigation. Our research indicates the potential quantum advantage with digital-analog gate models.

## 5 Acknowledgments

We thank Phil Lotshaw for constructive feedback on the manuscript. C.-C. Joseph Wang and Ryan Bennink acknowledges the support by the DOE Office of Science, Office of ASCR, under FWP No. ERKJ354.

## References

- [1] N. Wiebe, D. Braun, and S. Lloyd, Phys. Rev. Lett., 109:050505, 2012.
- [2] M. Schuld, I. Sinayskiy, and F. Petruccione, Phys. Rev. A., 94:0222342, 2016.
- [3] Y. Liu and S. Zhang, Theoretical Computer Science, 657:38-47, 2017.
- [4] Somma, Rolando D. and Subaşı, Yiğit, PRX Quantum, 2:010315, 2021.
- [5] Paine, Annie E. and Elfving, Vincent E. and Kyriienko, Oleksandr, Phys. Rev. A, 107:032428, 2023.
- [6] J. Preskill, Quantum, 2:79, 2018.
- [7] Cerezo, M., Arrasmith, A., Babbush, R. et al., Nat. Rev. Phys, 3:625–644, 2021.
- [8] E. Farhi, J. Goldstone, and S. Gutmann. A quantum approximate optimization algorithm. arXiv preprint quant-ph/1411.4028, 2014.
- [9] Grimsley, H.R., Economou, S.E., Barnes, E. et al. An adaptive variational algorithm for exact molecular simulations on a quantum computer. Nat. Commun., 10:3007, 2019.
- [10] Suguru Endo, Zhenyu Cai, Simon C. Benjamin, and Xiao Yuan, Hybrid Quantum-Classical Algorithms and Quantum Error Mitigation, J. Phys. Soc. Jpn, 87:023002, 2018.
- [11] Xiaosi Xu, Simon C. Benjamin, and Xiao Yuan, Variational Circuit Compiler for Quantum Error Correction, Phys. Rev. Applied, 15:034068, 2021.
- [12] Jacob Biamonte, Phys. Rev. A, 103:L030401, 2021.
- [13] Lennart Bittel and Martin Kliesch, Phys. Rev. Lett., 127:120502, 2021.
- [14] S. Ashhab, Phys. Rev. Research, 4:013091, 2022.
- [15] Cruz, D., Fournier, R., Gremion, F., Jeannerot, A., Komagata, K., Tasic, T., Thies-brummel, J., Chan, C.L., Macris, N., Dupertuis, M.-A. and Javerzac-Galy, C., Adv. Quantum Technol., 2:1900015, 2019.
- [16] D. Sierra-Sosa, M. Telahun and A. Elmaghraby, "TensorFlow Quantum: Impacts of Quantum State Preparation on Quantum Machine Learning Performance," in IEEE Access, vol. 8, pp. 215246-215255, 2020, DOI: 10.1109/ACCESS.2020.3040798.
- [17] Numerical Recipes. The Art of Scientific Computing, 3rd Edition, 2007, ISBN 0-521-88068-8. (C++ code)5-A. and Javerzac-Galy, C., Adv. Quantum Technol., 2:1900015, 2019.
- [18] Anupam Mitra, Michael J. Martin, Grant W. Biedermann, Alberto M. Marino, Pablo M. Poggi, and Ivan H. Deutsch Phys. Rev. A, 101:030301(R), 2020.
- [19] Michael J. Martin, Yuan-Yu Jau, Jongmin Lee, Anupam Mitra, Ivan H. Deutsch, Grant W. Biedermann, arxiv preprint quant-ph/2111.14677, 2021.
- [20] S. Debnath, N. M. Linke, C. Figgatt, K. A. Landsman, K. Wright, and C. Monroe, Nature, 536:63-66, 2016.
- [21] Barreiro J, Müller M, Schindler P, Nigg D, Monz T, Chwalla M, Hennrich M, Roos C F, Zoller P and Blatt R, Nature, 470:486 2011.
- [22] M Müller, K Hammerer, Y L Zhou, C F Roos , and P Zoller, New Journal of Physics, 13:085007, 2011.
- [23] Graham, T.M., Song, Y., Scott, J. et al. Multi-qubit entanglement and algorithms on a neutral-atom quantum computer. Nature, 604:457–462, 2022.

- [24] Bluvstein, D., Levine, H., Semeghini, G. et al. , *Nature*, 604:451–456, 2022.
- [25] Nielsen, M. A., and Chuang, I. L. (2011). *Quantum Computation and Quantum Information: 10th Anniversary Edition*. Cambridge University Press.
- [26] Peter Bruce and Andrew Bruce, *Practical Statistics for Data Scientists*, O'Reilly Media, Inc., First Edition, 2017.
- [27] Tasio Gonzalez-Raya, Rodrigo Asensio-Perea, Ana Martin, Lucas C. Celeri, Mikel Sanz, Pavel Lougovski, and Eugene F. Dumitrescu, *PRX Quantum*, 2:020328, 2021

## A Proof of cost function from measurement

$$\begin{aligned}
|\Psi_0\rangle &= \frac{1}{\sqrt{2}} \sum_{l',m'} x_{l'm'} \cos \phi_{m'} |l'm'\rangle, \\
\hat{M} &= \sum_{l'',m''} \sum_{l''',m'''} |l''m''\rangle \langle l'''m'''|, \\
\hat{M}|\Psi_0\rangle &= \frac{1}{\sqrt{2}} \sum_{l',m'} \sum_{l'',m''} \sum_{l''',m'''} x_{l'm'} \cos \phi_{m'} \langle l''m'''|l'm'\rangle |l''m''\rangle,
\end{aligned}$$

Using the orthogonality relation,

$$\begin{aligned}
\langle l''m'''|l'm'\rangle &= \delta_{l''m'''=l'm', 0} \\
&= \frac{1}{\sqrt{2}} \sum_{(l'',m''')} \sum_{(l''',m''')} x_{l'm'''} \cos \phi_{m'''} |l''m''\rangle, \\
\langle \Psi_0 | \hat{M} | \Psi_0 \rangle &= \frac{1}{2} \sum_{l'',m'''} \sum_{l,m} \sum_{l'',m''} x_{lm} x_{l''m'''} \cos \phi_m \cos \phi_{m'''} \langle lm | l''m''\rangle \\
&= \frac{1}{2} \sum_{l'',m'''} \sum_{l'',m''} x_{l''m''} x_{l''m'''} \cos \phi_{m''} \cos \phi_{m'''} \\
&= \frac{1}{2} \sum_{l''} \sum_{m''} x_{l''m''} x_{l''m'''} \cos \phi_{m''} \cos \phi_{m'''} \\
&= \frac{1}{2} \sum_l (\sum_m x_{lm} \cos \phi_m)^2,
\end{aligned} \tag{51}$$

Q.E.D.

## B Measurement feasibility

By the measurement outcome from a perfectly trained model with less noisy data and good independent features selected in Eq. (16), we expect vanishing measurement results  $\text{Pr}_{\text{perfect}}$  from a perfect destructive interference since the predicted response  $\hat{y}_{l \in \{0, 1, 2, \dots, L-1\}}$  agrees with the actual response  $y_l$  in comparison with models which are not well trained.

For a poor model, what the model learned is the vanishing weights  $\bar{W}_m$ . If the response variable is standardized with subtraction from its mean value, we expect the standardized bias term is zero and we expect a finite outcome from Eq. (16) only contributed from the standardized response data  $y_l^S$  as

$$\text{Pr}_{\text{Poor}} \propto \sum_l (y_l^S \cos \phi_y)^2. \tag{52}$$

For the worst model, we expect the signs of the weights are all wrong and a much larger probability outcome is expected as

$$\text{Pr}_{\text{Worst}} \propto \sum_l (2y_l^S \cos \phi_y)^2. \tag{53}$$

We can define the goodness model metrics  $G_M$  for the trained model as  $G_M \equiv 1 - \text{Pr}_{\text{M}}/\text{Pr}_{\text{Poor}}$

$$G_M : \begin{cases} = 1 & \text{Perfect} \\ = 0 & \text{Poor} \\ = -3 & \text{Worst} \end{cases}. \tag{54}$$

For the worst circumstance where the best estimation of the weight are wrong in signs, the goodness for the worst model  $G_{\text{Worst}}$  will approach the value  $-3$ . This will be the case when the optimizer is not set up correctly to find the minima but finding the maxima or the sign for rotational angle for the response variable is not well taken off. For any meaningful training results, the goodness metrics should be in the range  $G_M \in (0, 1]$ .

Notice that the model metrics  $G_M$  is independent of any normalization convention in the algorithm. To conclude if the measurement outcome is feasible, we can estimate what is needed for the measure probability  $\text{Pr}_{\text{Poor}}$  to be resolved in lab experiments. In terms of the standardized response variable  $y_l^S$  after global normalization, the probability  $\text{Pr}_{\text{Poor}}$  can be expressed as

$$\text{Pr}_{\text{Poor}} = \frac{1}{R^2} \sum_l (y_l^S \cos \phi_y)^2, \quad (55)$$

where  $R^2$  is the global normalization factor after state preparation. In terms of typical column standardized classical data, the global norm  $R^2$  is given by

$$R^2 = \sum_l y_l^S {}^2 + \sum_{lm} x_{lm}^S {}^2 = \sigma_{y^S}^2 + \sum_m \sigma_{x_m^S}^2, \quad (56)$$

in which the number of row is given by  $L$ , the variance for the input variable  $x_m^S$  with column  $m$  is given by  $\sigma_{x_m^S}^2$  and the variance for the response variable  $y$  is given by  $\sigma_{y^S}^2$ . Finally, we can arrive at the following expression for the probability  $\text{Pr}_{\text{poor}}$  as

$$\begin{aligned} \text{Pr}_{\text{Poor}} &= \cos^2 \phi_y \frac{\sigma_{y^S}^2}{\sigma_{y^S}^2 + \sum_m \sigma_{x_m^S}^2} \\ &= \cos^2 \phi_y \frac{1}{1 + F}, \end{aligned} \quad (57)$$

in which the total variance of all  $M$  features is given by  $\sum_m \sigma_{x_m^S}^2$ , the variance of the response variable is given by  $\sigma_{y^S}^2$ , and the relative variance ratio factor  $F$  between all features and the response is defined by  $F \equiv \sum_m \sigma_{x_m^S}^2 / \sigma_{y^S}^2$ .

To maximize observable success probability outcome, we expect to work at the parameter regime  $|\cos \phi_y|$  to be close to one with the rotational angle  $\phi_y \bmod 2\pi$  close to  $0, \pi$ . For the relative variance ratio factor  $F$ , it scales with number of the encoded feature  $M$ . Therefore, we expect the success probability  $\text{Pr}_{\text{Poor}}$  to scale inversely as the number of features  $M$ . For a perfect model built, there should be a destructive interference leading to zero observable probability  $\text{Pr}_M$ . To be distinguishable from  $\text{Pr}_{\text{Poor}}$  in probability measurement resolution  $\epsilon \ll 1$  which is about a few percent, the number of features cannot be too large, that is, the number of the feature  $M$  is upper bounded by  $1/\epsilon$  ( $M < \epsilon^{-1}$ ) as our measurability criteria. For a classical data set with  $K$  data entries, that is,  $K \approx LM$ , the criteria changes to  $K/L < \epsilon^{-1}$ . Therefore, a tall table ( $L \gg M$ ) with limited features are possible to be measured, which further strengthens the importance of feature selection in quantum machine learning.

## C Hardware implementation

In cold-ion hardware, the native gates include arbitrary one-qubit Pauli rotational gates and the two-qubit gate XX [20]. The controlled phase (CPH) gate and the controlled NOT (CNOT) gates can be realized using the XX gate in conjunction with 1-qubit Pauli

rotations. The  $H$  gate can be decomposed as  $R_X(\pi)R_Y(\pi/2)$  also in the platform. (Note that arbitrary 1-qubit gates plus any entangling 2-qubit gate constitute a universal set, so the Rydberg platform implements a universal set.)

In the Rydberg-atom platform [23], any rotation in the Bloch sphere can be implemented and the native two-qubit gate is ZZ. The CNOT gate can also be decomposed in this platform as  $(I \otimes H)C_Z(I \otimes H)$  where the controlled  $Z$  gate  $C_Z$ , which is a special case for the controlled phase gate, is enabled by Rydberg states. The CPH gate can be decomposed in principle in terms of the CNOT gate with a one-qubit rotational gate [25].

The specifics of CPH gates vary with encoding schemes. For the one-hot amplitude encoding, the factorization of controlled two-body Pauli rotations  $U_C^j$  along an axis is required. Typically, this can be achieved in a preferred Pauli  $Z$  axis in a particular platform up to a single qubit rotation from a native axis to the  $Z$  axis. For example, the native axis for cold ion would be Pauli  $X$  and the native axis for the Rydberg atom will be Pauli  $Z$ . The multi-qubit controlled phase gate can be implemented for the native Pauli  $Z$  axis as  $U_C^{(m)} = \prod_j \exp(-i\phi_m \frac{Z_A - I_A}{2} \otimes \frac{Z_j - I_j}{2})$ . Equivalently, it can also be decomposed locally as

$$U_C^{(m)} = \prod_j e^{-i\frac{\phi_m}{4} Z_A \otimes Z_j} e^{+i\frac{\phi_m}{4} Z_A \otimes I_j} e^{+i\frac{\phi_m}{4} I_A \otimes Z_j} e^{-i\frac{\phi_m}{4} I_A \otimes I_j}, \quad (58)$$

in which the last unitary exponential factor is the idler unitary operator, which is state independent and can be dropped. By digital 1-local and 2-local gate operation, the time complexity for each feature is of  $O(LM)$ . With  $M$  features, the time complexity will be of  $O(LM^2)$ . For digital globally-addressed analogue gate operation on each feature, the time complexity is greatly reduced to be  $O(1)$  and scales as  $O(M)$  with globally addressed analog gates. With fully-programmable global analogue gate operation with all features and the involved commutative Pauli operators,  $\prod_m U_C^{(m)}$  can be fused into a global unitary, and therefore the time complexity can be minimized to  $O(1)$ . This illustrates the relevance of computing paradigms to time complexity.

For the native  $X$  axis, we need to apply Pauli  $Y$  rotation  $R_{Y_{A,j}}(-\pi/2)$  to each physical qubit state in  $U_C(\phi_m)$  as

$$\begin{aligned} U_C^{(m)} = & \prod_j R_{Y_A}(+\pi/2) R_{Y_j}(+\pi/2) e^{-i\frac{\phi_m}{4} X_A \otimes X_j} R_{Y_j}(-\pi/2) R_{Y_A}(-\pi/2) \\ & \otimes R_{Y_A}(+\pi/2) e^{+i\frac{\phi_m}{4} X_A \otimes I_j} R_{Y_A}(-\pi/2) \\ & \otimes e^{+i\frac{\phi_m}{4} I_A \otimes X_j}, \end{aligned} \quad (59)$$

in which the digital and local decomposition has arrived. For the controlled phase gate for state preparation, the gate needs to be applied to each qubit reserved for the data registry.

For the compressed binary encoder, the controlled phase gates are more complicated to implement, and we suggest the application of a global entanglement gate, Mølmer-Sørensen (MS) gate with a ancilla qubit, to achieve the quantum logic gate [22]. The MS gate unitary operator in trapped cold ions is typically expressed as

$$U_{MS}(\theta_{MS}, \phi) = \exp(-i\frac{\theta_{MS}}{4}(\cos(\phi)S_X + \sin(\phi)S_Y)^2), \quad (60)$$

in which  $S_{X,Y} = \sum_i X_i, \sum Y_i$  are the collective Pauli-operators. With the help of an ancilla qubit, Pauli-string operation along a Pauli-axis  $X, Y$  can be enabled by choosing the value and the sign of the phase  $\phi$  to be  $0, \pi$ . For  $\phi = (0, \pi)$ ,  $U_{MS} = (U_{MS}^X(\theta_{MS}, \phi = 0), U_{MS}^Y(\theta_{MS}, \phi = \pi))$ . The angle  $\theta_{MS}$  can be used to tune the strength of the rotation

for the MS gate where the exhaustive implementation has been listed in Table 1 in the reference. Notice that any discrepancy between the algorithm we develop can be easily adjusted to the native preferred axis for any platform after global rotation without many difficulties. The same comments hold as the one-hot encoder for the state preparation with controlled phase gates based on MS gate. For Rydberg atoms, the research on MS gates for two atoms and multiple atoms are just in their infancy [18, 19].

For well-connected qubits, the multi-controlled phase gates would be sufficient to implement with only one ancilla in principle, especially when the connectivity is close to infinitely long-ranged. Partly the practicality of the implementation is limited by the range of the phase gates that can be applied uniformly across physical qubits. To add the fine programmable capability, individual and segmented digital addressing with the global entangled MS gate and local gates are possible. For example, for cold ions in a one-dimensional linear Paul trap and a two-dimensional Penning trap, the ions are mostly uniformly distributed with long-ranged Ising interactions at the center of the trap. Therefore, it would be wise to select the ions away from the edges of the trap as the data register to reduce sophisticated waveform engineering. Due to this controlled scalability limitation, we anticipate machine learning limited to a certain number of qubits which limits the amount of training data that can be encoded for learning currently.